Modelling Simple Feature Creation in Selective Laser Sintering

Ryder G. J., Berzins M., Childs T. H. C.
University of Leeds

A two dimensional finite difference thermal sintering model has been created to describe the Selective Laser Sintering process(SLS). It includes thermal property variation with position and temperature, and especially adaptive meshing to refine information in regions of high temperature gradients. It has been used to predict density and temperature in both single and multi layer sintering operations, corresponding to experimental results. This paper will present comparisons of theory and experiment for the SLS of simple geometries such as blocks, steps, and cylinders.

INTRODUCTION

Earlier work [1-3] has reported the advances in the modelling of the sintering process at Leeds. Initial thermal modelling with classical moving heat source theory has been superseded by finite difference numerical methods using adaptive meshing which is the key feature of the software VLUGR2 [4]. The work is currently restricted to two dimensional modelling. The work presented here takes this work a step further. Bonus Z (Z+), curl and growth are well reported [2,3] as the limiting accuracy associated with the sintering process. Z+, and growth are also known to be related to a build up of excess heat within the system. At least two types of curl have been distinguished. The first is as a result of the thermal stresses built up within a material as it shrinks, resulting in the curling of the whole layer or part, and will be referred to as 'major curl'. The second, that is confined to the very edges of a part, seems to be as a result of the original sintering of the powder, and will be known as minor curl. It is minor curl that can be illustrated in this work.

The present generation of SLS machines does not have the facility to vary energy input to the powder bed point to point. Some of the problems described above are orientation and part geometry dependent. Better understanding could lead to a reduction of the problems through the more flexible control of the laser operating parameters. The aim of this work is to develop strategies that will be applicable to future generations of sintering machines.

THEORY

Figure 1, [1], shows the simplified model of the rastering laser that has been introduced to describe SLS in two dimensions. As described in [1] when scan spacing, s < beam diameter, d and if the cycle time 2w/U is less than the time d^2/κ for heat to diffuse d (where κ is the thermal diffusivity), the laser spot, with power P, may be replaced by a rectangular blade source of side d x w, of power Q per unit area, sweeping across the block with speed V in the x direction where

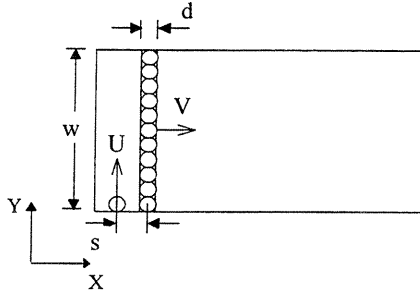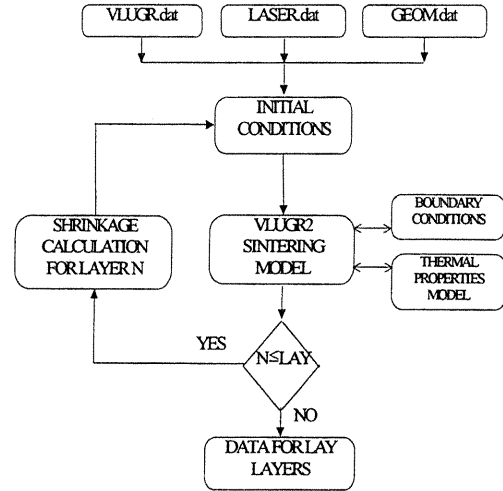$$Q = \frac{P}{Usd} \tag{1}$$

Figure 1: Scanning model.

Figure 2: Flow chart of AMP2 model.

Figure 1 describes the laser tracking over a simple rectangular patch, to sinter one layer of a rectangular part. It may be thought of as one slice of a three dimensional part, in which shape can be created by displacing one layer in the X direction relative to the last and/or by changing the length of the layer in the X direction. This is the focus of this paper. A flow chart of the multi-layer computer model is shown in figure 2. The model has been called AMP2, or Accurate Multi-Layer Prediction model in 2D, and has been used in this report to generate simple geometries such as blocks, steps and cylinders that can be compared with experimental data. In this paper numerical results from AMP2 will mainly be discussed, and initial comparisons will be made with experimental work.

At the start of the run three external files are opened and their contents read into the program. VLUGR.dat contains information relevant to the running of the VLUGR2 software: domain data, tolerance data, and Partial Differential Equation(PDE) data. GEOM.dat contains the geometry data including the scan spacing, scan vector length, and the start and end coordinates of each layer. Finally LASER.dat contains the LASER data: laser power, laser spot size, and the scan speed. This data is used to create the specific sintering model within VLUGR2 which then calculates the temperature/time history and the sintering behavior of the model.

The model is based around two major PDEs, the heat conduction equation (2) and the viscous sintering equation (3) in which ε is the void fraction

$$\rho C_p \frac{\partial T}{\partial t} = K\left(\frac{\partial^2 T}{\partial x^2} + \frac{\partial^2 T}{\partial y^2}\right) + \frac{\partial K}{\partial T}\left(\left(\frac{\partial T}{\partial x}\right)^2 + \left(\frac{\partial T}{\partial y}\right)^2\right) + \left(\frac{\partial K}{\partial x}\frac{\partial T}{\partial x}\right) + \left(\frac{\partial K}{\partial y}\frac{\partial T}{\partial y}\right) \quad (2)$$

$$-\frac{\partial \varepsilon}{\partial t} = k'\left(\varepsilon - \varepsilon_\infty\right) \quad (3)$$

where $k' = A\exp\left(-\dfrac{B}{RT}\right)$ (4)

An important feature of equation (2) is that it retains terms in conductivity varying with position and temperature, as described briefly in ref(3). A difference from earlier papers [1] is that it does not contain a convection (moving heat source) term. In the present treatment, the moving heat source is treated as a moving flux boundary condition. The temperature/time history of the powder is calculated as the laser passes by. The void fraction variation described by equation (3) is calculated simultaneously, and this feeds back into the heat conduction equation via the variation of thermal conductivity with position. While the void fraction is calculated simultaneously, the overall shrinkage (depression of the powder surface) that takes place as a result of the solidification of the powder is calculated as a post processing operation, [1,2]. Because this is the case care is needed in the interpretation of the conductivity terms in eqn (2).

Equation 2 does not contain the latent heat terms that are required to model crystalline polymers. At this stage the model is still restricted to the modelling of amorphous polymers such as polycarbonate. For polycarbonate from Nelson [5],

$$C_p = 935 + 2.28T \quad \text{(J/Kg)} \tag{5}$$

while the thermal conductivity model is stated as

$$K_{solid} = 0.0251 + 0.0005T \quad \text{(W/mm-K)} \tag{6}$$

In previous work [2,3], a simplified expression was used for the conductivity of the powder or partially sintered material

$$K_{powder} = K_{solid}(1 - \varepsilon) \tag{7a}$$

As a result of measurements still in progress the following is now preferred

$$K_{powder} = K_{solid}(1 - \sigma\varepsilon) \tag{7b}$$

with a value of $\sigma = 0.5$. This empirical expression, valid for the range of void fraction seen in SLS, is still substantially simpler than the expression used by Nelson [5,6]. From equation 7b the temperature and spatial variation of K in equation 2 becomes

$$\frac{\partial K}{\partial T} = (1 - \sigma\varepsilon)\frac{\partial K_{solid}}{\partial T} \quad , \qquad \frac{\partial K}{\partial n} = -\sigma K_{solid}\frac{\partial \varepsilon}{\partial n} \tag{8}$$

where here n represents either the x, or y axes. Notice here that the K is the conductivity of the solid, while the K prefixing the first term on the right hand side of equation 2 and ρ on the left hand side is that of the initial bed density.

The sintering prediction is performed in two distinct operations. The first is to calculate the sintering behavior of the first single layer, in which the phenomenon of Z+ is observed. It is this operation that has been reported previously [3]. The second is the sintering of the subsequent layers whose sintering behavior is affected by the presence of the immediately previous layer. The effect of this previous layer is to conduct the heat away from the sintering region more quickly resulting in a reduced sintering depth. AMP2 eliminates the computational expense of a large number of layers by only modelling two layers at a time, the layer being sintered and the immediately previous layer.

By sintering behaviour is meant the calculation of void fraction with position, from equations 2 and 3. The shrinkage of the layer is then calculated. Information of the density and shrinkage of the first layer are re-entered as initial conditions to the sintering calculation of the next layer. Once all layers have been modelled the complete layer data is entered into VLUGR2 and this data is the dump to an external file. Currently a single average run with P=11W, s=0.15mm, U=1190 mm/s, creating a part length of 5mm and 10 layers thick can take 30 hours using an average number of 35,000 grid points.

Two major geometries have been modelled using the AMP2 model: blocks and steps. A brief examination of cylinders has also been undertaken, but only a preliminary report of this is included here. The blocks are the simplest geometry. A simple diagram of the three dimensional geometry is shown in figure 3. This is in fact the geometry that was built within the SLS machine, the numerical model looked at the cross section of this part along the length, L. The step and cylinder geometries are likewise shown in figure 3.
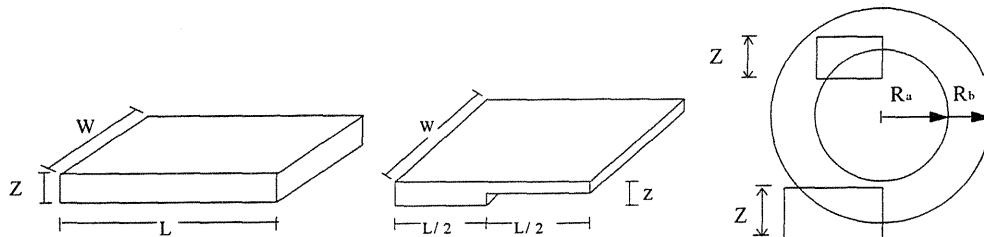

Figure 3: Block, step and cylinder geometries.

Only part of the cylinder geometry is modelled. The difference of scale between the overall size of the object and the area being sintered coupled with the memory requirements of the VLUGR2 software make it difficult to model the entire geometry. Therefore only those regions that are of interest are modelled. Region 1, the bottom of the cylinder, is prone to Z+ on the bottom layer causing the geometry to become oval. Region 2, the top inside diameter, is known also to suffer this type of problem resulting in a flattening of this inside diameter.

The AMP2 model as presented here allows the user to control the sintering variables of laser power, scan spacing, scan vector length, dwell time, laser spot diameter, and laser scan speed. By manipulating these variables it is possible to model simple two dimensional sintering strategies.

EXPERIMENTATION

The numerical calculations from AMP2 have been compared with two types of tests: calibration experiments and ones in which blocks, and steps were created.

The calibration experiments have been reported before. Simple rectangular blocks were built with powers from 4 to 19Watts, scan speeds from 51 to 1206mm/s and scan spacings from 0.08 to 0.41mm. The densities of these parts were measured and the average layer density calculated. The AMP2 predictions are compared with this.

Experimental pieces ten layers thick corresponding to powers of 6, 11, and 22 Watts, s=0.15mm, w=25mm, and U=1190mm/s were built in the SLS machine. Once built these were mounted for microscopic examination in EPOFIX cold setting resin using the vacuum impregnation technique. These were then ground, polished and photographed in order that they could be compared with the numerical results obtained from AMP2.

NUMERICAL AND EXPERIMENTAL RESULTS

Figure 4 shows the calibration tests. Figure 4a shows calculated layer thickness for the first, second and third layer of a part. The Z+ phenomenon is clearly visible as a greater thickness of the first few layers; the results are in accord with experiments [3]. Figure 4b shows the variation of the average layer density, once the steady state thickness of the layer has been obtained. The error bars mark experimental results, the line is the prediction from AMP2.
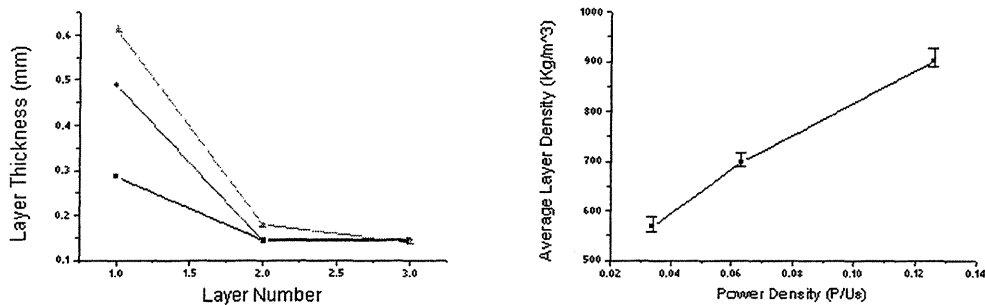

Figure 4: Multi layer model calibration data (a) layer thickness vs. layer number ▲ 22W ■ 11W ● 6W (b) layer density vs. power density for experiment and current AMP2 model.

Figure 5: Single layer after shrinkage calculation.

Contour plots of the densification data obtained from VLUGR2 are created using the UNIMAP software, a component of the UNIRAS suite. At this stage of the research they are a geometrical representation only: they show only the distinction between solid and powder. Figure 5 shows a single layer output from AMP2 after the shrinkage post processor has been applied. In this case it was built at P=11W, U=860mm/s, s=0.203mm. The cause of minor curl can clearly be seen on the downward facing surface, the rounding of the edge caused by the initial sintering of the layer.

Figure 6 shows AMP2 results for 10 layer thick block (a, close up d) and step (b, close up e) models built at 6W power (c defines the grey scales). The models, nominally 1.25 mm thick, are actually 1.3 mm as a result of only a small amount of Z+ creation. The model predicts some unsintered powder between each layer. In the step model, each of the top five layers shows a small step or change of level as it crosses over the edge of the step.
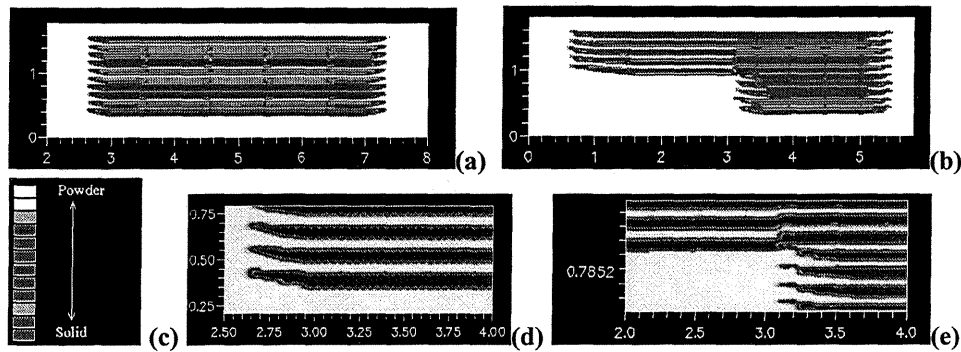

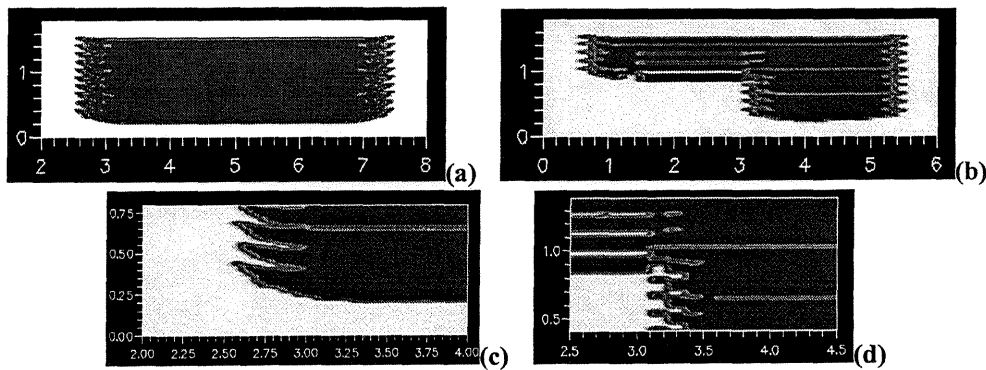Figure 6: Geometry data for 6W, all dimensions mm.

Figure 7: Geometry data for 11W, all dimensions mm.

Figure 7 shows the 11W power block and step AMP2 output. total thickness of the block has increased to 1.4 mm due to greater Z+. Little unsintered powder remains inside the model. In figure 7d, the change of the upper part of the model's layer level at the step edge cross-over can still be seen.

At 22W (figure 8), the block appears fully dense. It has become 1.7 mm thick, due to large Z+ which also gives a marked rounding (curl) to the bottom surface.
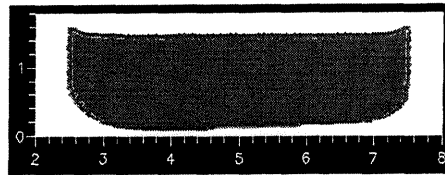

Figure 8 : Block geometry at 22Watts, all dimensions mm.

Figure 9 shows region 1 of the 11W AMP2 cylinder model as described in the theory section. The thickness of the 10 layers is 1.45 mm, corresponding to 0.2 mm Z+. The leading (left-hand) edge is rippled. This is the same effect as seen in the step models (figures 6d and 7d) in which layer level changes as it passes over the edge of a previously sintered layer.
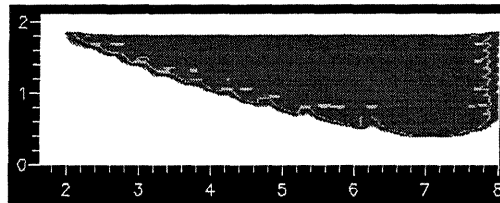

Figure 9: Cylinder multi layer model, region 1, all dimensions mm.

Initial experimental results are shown in figure 10. Part a shows the structure of a single layer block built at 11W: it shows the same curl as in figure 5. Part b is a 10 layer block to be compared with figure 7a: it is more clearly layered than is figure 7a; also the left-hand edge is clearly not as square as in figure 7a. Part c is a detail of a step to be compared with figure 7d: the change of level of a layer as it crosses the step edge can be seen. Part d is a 10 layer block built at 22W for comparison with figure 8. The large circular black regions are closed pores not predicted by the model and different in structure from parts made at 11W.

DISCUSSION AND CONCLUSION

The 2D AMP2 program, including variation of thermal conductivity with position and temperature and with an improved expression for thermal conductivity (equation 7b) accurately predicts part density and bonus Z (Z+). It is starting to be used to model simple features in comparison with experiments and shows promise of being able to guide, after further post-processing development, strategies for more accurate sintering to shape. involving variable power according to part geometry. However some features on even simple shapes, such as the non-square edge in figure 10c, show the equal importance of being able to model post-sintering distortion due to viscous relaxation of internal stresses. Experimental studies also show that the sintering process itself, in extreme conditions such as the high laser power in figure 10d, is more complicated than suggested by the simple rate model of equation 3.
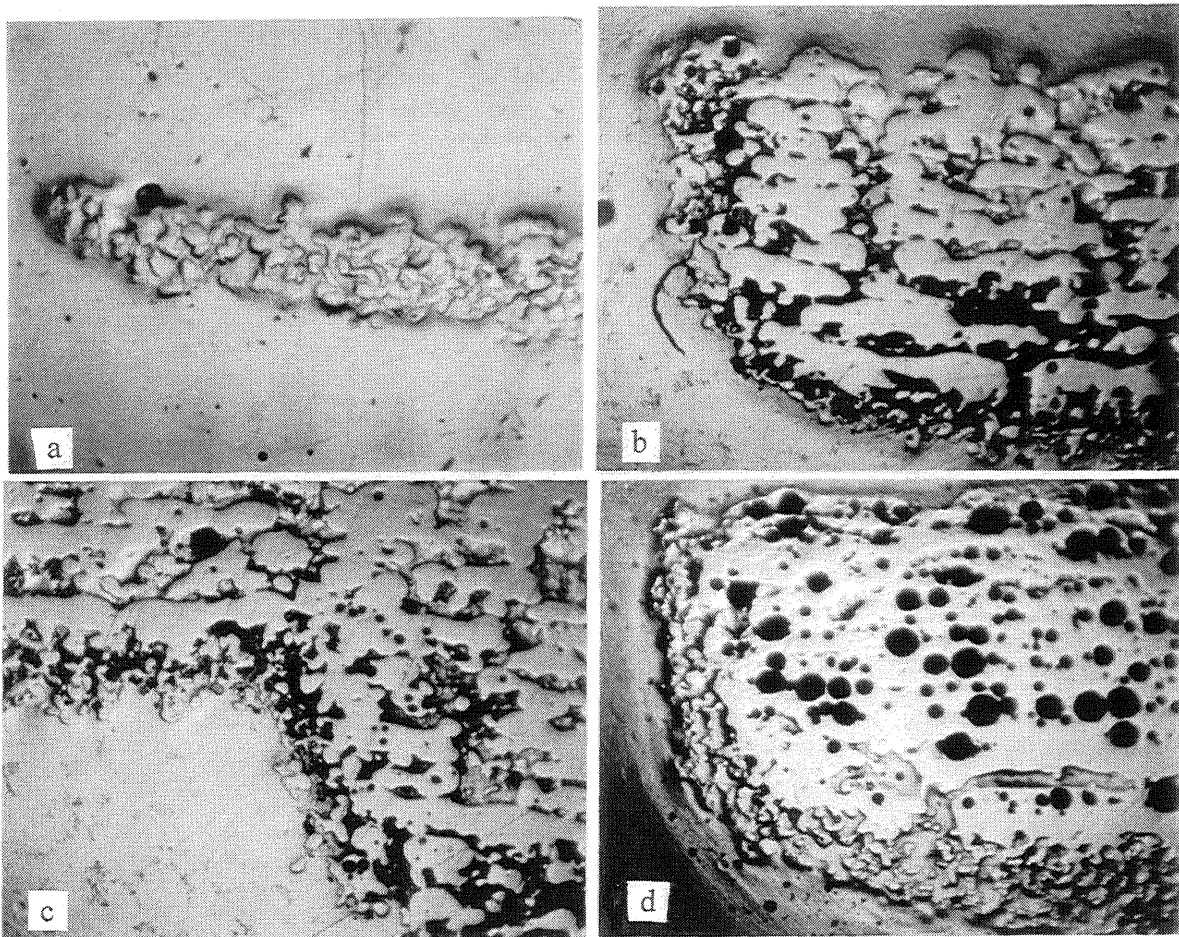
Figure 10. Microsections of parts built at 11W (a to c) and 22W (d), as described in text.

ACKNOWLEDGEMENTS

REFERENCES

1. Childs, T. H. C. et al., 1994, Selective Laser Sintering of Polycarbonate at Varying Powers, Scan Speeds and Scan Spacings, Proc. 5th SFFF Symposium, 356-363, University Austin Texas.
2. Berzins, M., Childs, T. H. C., et al., 1995, Densification and distortion in Selective Laser Sintering of Polycarbonate, , Proc. 6th SFFF Symposium, 196-203, University Austin Texas.
3. Berzins, M., Childs, T. H. C., Ryder, G. J., The Selective Laser Sintering of Polycarbonate, Annals CIRP 44/1 (1996), to be published.
4. Blom, J. G. and Verwer, J. G., 1993, VLUGR2: A Vectorisable Local Uniform Grid Refinement Code for PDEs in 2D, to appear in ACM T.O.M.S. September 1996.
5. Nelson, J. C. et al., 1993, Model of the Selective Laser Sintering of Bisphenol-A Polycarbonate, Ind. Eng. Chem. Res., 32: 2305-2317.
6. Yagi, S., Kuni, D., Studies on Effective Thermal Conductivities in Packed Beds, AIChE J., 1957, 3, 373-381.